Check for updates

Received: 1 December 2023 | Revised: 8 February 2024 | Accepted: 20 February 2024

DOI: 10.1002/aoc.7433

FULL PAPER

Applied Organometallic Chemistry WILEY

Pd(II) and Pt(II) saccharinate complexes with two phosphine derivatives: Synthesis, anticancer and antiangiogenic activities

Ceyda Icsel[1] | Veysel T. Yilmaz[1] | Muhittin Aygun[2] | Merve Erkisa[3] | Engin Ulukaya[4] | R. Okan Akar[4]

[1]Department of Chemistry, Faculty of Sciences, Karadeniz Technical University, Trabzon, Turkey

[2]Department of Physics, Faculty of Sciences, Dokuz Eylul University, Izmir, Turkey

[3]Faculty of Medicine, Istanbul Health and Technology University, Istanbul, Turkey

[4]Department of Clinical Biochemistry, Medical School of Istinye University, Istanbul, Turkey

Correspondence
Ceyda Icsel, Department of Chemistry, Faculty of Sciences, Karadeniz Technical University, 61080 Trabzon, Turkey.
Email: cydyilmaz@ktu.edu.tr

As clinically used anticancer Pt(II) drugs have severe side effects, there is a growing interest for new metal complexes with great potential for cancer therapy. The current work aimed to prepare and characterize new Pd(II) and Pt(II) saccharinate (sac) complexes bearing pyridyl- and benzyldiphenylphosphines (PPh_2Py and PPh_2Bz, respectively), *cis*-$[Pd(sac)_2(PPh_2Py)_2]$ (**1**), *cis*-$[PtCl(sac)(PPh_2Py)_2]\cdot 0.5DMF$ (**2**), *cis*-$[Pd(sac)_2(PPh_2Bz)_2]\cdot DMF$ (**3**) and *trans*-$[PtCl(sac)(PPh_2Bz)_2]$ (**4**) as promising anticancer and antiangiogenic drugs. The anticancer activity of the complexes was screened against seven cancer cell lines including HCT116 (colon), HepG2 (liver), MDA-MB-231 (breast), PANC-1 (pancreatic), A549 (lung), C6 (glioma), DU145 (prostate) and normal human lung epithelial cells (BEAS-2B). **1** and **2** did not show biological activity below 20 μM at 48 h, whereas **3** and **4** displayed significant cytotoxic effect on the cancer cells. **4** was the most potent complex (IC_{50} = 2.2–12.1 μM) and displayed much greater cytotoxicity than cisplatin in all the cancer cell lines. **4** caused apoptosis in HCT116 cells as evidenced by annexin V positivity and caspase 3/7 activity assays. Furthermore, the inhibition of antiapoptotic Bcl-2 proteins by the complex suggested the intrinsic apoptosis. In addition, **4** greatly enhanced generation of intracellular reactive oxygen species (ROS) and consequently caused remarkable DNA double-strand breaks in HCT116 cells. Moreover, the chick chorioallantoic membrane (CAM) assay was used to evaluate antiangiogenic potential of **4**. The complex effectively inhibited angiogenesis at a dose of 50 ng, suggesting it as a promising multi-targeted agent for antiangiogenic cancer treatment.

KEYWORDS

antiangiogenics, anticancer activity, cell apoptosis, palladium(II) and platinum(II) complexes, X-ray structures

1 | INTRODUCTION

Saccharin (sacH, 1,1-dioxo-1,2-benzothiazol-3-one or benzosulfimide) is a well-known non-nutritive synthetic sweetener. Its deprotonated form (sac) received great interest as a versatile polyfunctional ligand in coordination chemistry. The sac ligand displays monodentate, bidentate and tridentate chelating and bridging coordination modes.[1]

Cisplatin, oxaliplatin and carboplatin are widely used drugs to treat cancer. However, due to severe side effects

 © 2024 John Wiley & Sons Ltd.

and drug resistance, research has been extended to other Pt(II) complexes. Over the past decade, a great number of Pt(II) complexes were extensively synthesized and evaluated in vitro and in vivo, some of them exhibiting considerable anticancer activity.[2–10] In addition, some Pd(II) complexes also demonstrated promising cytotoxic activity.[2,3,8,11–13] Studies showed that some mixed-ligand Pd(II) and Pt(II) complexes of sac exhibited promising anticancer activity.[14,15] In addition, in vitro and in vivo anticancer activities of a series of Pd(II) and Pt(II) complexes of sac with polypyridyl ligands synthesized by our research group were evaluated with encouraging results.[16–20] The metal complexes of sac with potent anticancer activity were briefly discussed in recent reviews.[2,3,11,21]

The synthesis and biological activity of phosphines and their metal complexes have long attracted the attention of researchers. The Pd(II) and Pt(II) sac complexes of phosphines (PPh_3 or $Ph_2PCH_2CH_2PPh_2$) were first reported in the late 1990s.[22] Because Pd(II) and Pt(II) complexes containing both sac and phosphine ligands are rare, we have therefore recently involved in the synthesis and anticancer potentials of Pd(II) and Pt(II) sac complexes of monophosphines[23–26] and diphosphines.[27,28] From a medicinal inorganic chemistry point of view, the presence of carbonyl and sulfonyl groups makes sac hydrophilic, which regulates the lipophilicity of the metal complexes. Moreover, such complexes may form strong hydrogen bonds with DNA via the hydrogen bond acceptor groups in sac.[23–28] As a results, sac greatly increases the potency of metal complexes and therefore is considered as a novel targeting ligand.[21] On the other hand, phosphine ligands with nonpolar groups modulate the lipophilicity of metal complexes and consequently enhance their bioavailability and cytotoxicity.[29] The alteration of the hydrophobic groups in tertiary phosphines greatly affects the biological activity of the respective metal complexes.

As continuation of our interest, the present study was planned to design and synthesize new biologically active Pd(II) and Pt(II) sac complexes (**1**–**4**) bearing two tertiary phosphine derivatives, PPh_2Py and PPh_2Bz (Scheme 1). The cytotoxicity of the complexes was screened against seven cancer (HCT116, HepG2, MDA-MB-231, PANC-1, A549, C6 and DU145) and normal (BEAS-2B) cell lines. Induction of apoptosis, generation of ROS and DNA double-strand breaks (DSBs) caused by the most potent complex (**4**) in HCT116 cells were carried out to elucidate the mode of cell death. Because compounds targeting angiogenesis have the potentials to be used in cancer treatment due to their inhibition of tumour growth and progression,[30] the antiangiogenic potential of **4** was evaluated by the CAM assay. The aim of the study is to develop a promising drug to be used in the antiangiogenic cancer treatment.

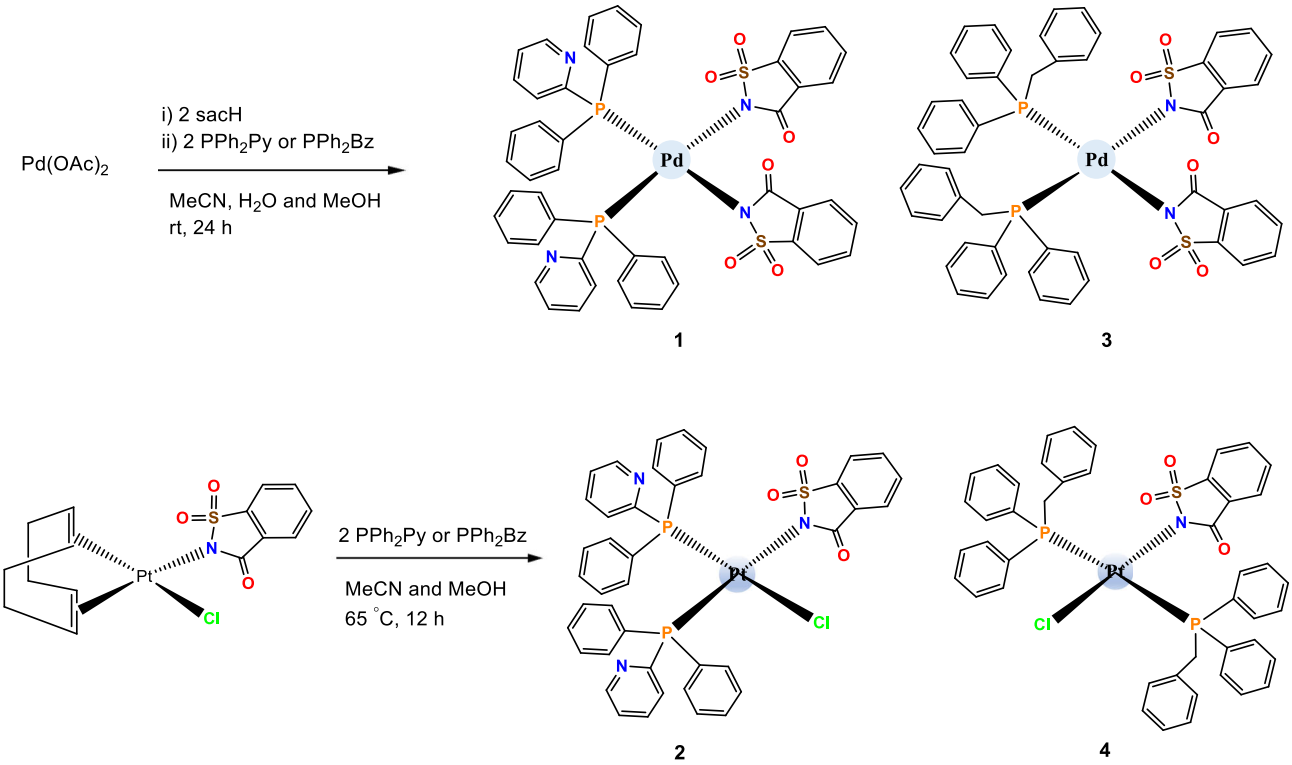

SCHEME 1 Schematic representation of general synthesis of Pd(II) and Pt(II) sac complexes (**1**–**4**) containing PPh_2Py and PPh_2Bz.

10990739, 0, Downloaded from https://onlinelibrary.wiley.com/doi/10.1002/aoc.7433 by Dokuz Eylul University, Wiley Online Library on [06/03/2024]. See the Terms and Conditions (https://onlinelibrary.wiley.com/terms-and-conditions) on Wiley Online Library for rules of use; OA articles are governed by the applicable Creative Commons License

2 | RESULTS AND DISCUSSION

2.1 | Synthesis and structural characterization

The Pd(II) complexes were synthesized by the reaction of $Pd(OAc)_2$ (palladium(II) acetate) with sacH in a molar ratio of 1:2 in an aqueous solution of acetonitrile (MeCN) at room temperature (rt). Then, the addition of 2 mol PPh_2Py and PPh_2Bz in methanol (MeOH) to the resulting solutions yielded complexes of **1** and **3**, respectively. Complexation of PPh_2Py and PPh_2Bz with Pt(II) to give **2** and **4** was carried out in MeCN at 65°C, using [PtCl(sac)(COD)] (COD = 1,5-cyclooctadiene) as a precursor.[31] In all the cases, the complexes were obtained in high yields and are highly soluble in the common organic solvents. Molar conductivity of the complexes in MeOH was low, indicating their non-electrolytic character.

The spectroscopic characterization data recorded for **1**–**4** are presented in Section 4 and Figures S1–S3. The IR bands appeared at 1015–990 cm^{-1} were assigned to the C—P stretchings of the phosphine ligands. The sharp bands in the region of 1680–1650 cm^{-1} were attributed to the ν(C═O) vibration of sac, and the medium to sharp absorptions in the region 1305–1245 and 1170–1150 cm^{-1} were due to $\nu_{as}(SO_2)$ and $\nu_s(SO_2)$ vibrations of the sulfonyl group of sac, respectively.[32] The ^1H, $^{13}C\{^1H\}$ and $^{31}P\{^1H\}$ NMR spectra displayed the characteristic resonances of the functional groups present in complexes **1**–**4** (Figure S2).

The ^1H NMR spectra revealed the signals of the aromatic protons of PPh_2Py, PPh_2Bz and sac as multiplets in the range of 9.05–6.50 ppm. The protons of the CH_2 group of PPh_2Bz in **3** and **4** appeared as a well-resolved doublets between 3.82 and 4.17 ppm. The signals centred around 165 and 140 ppm in the ^{13}C NMR spectra were characteristic to the C═O and C—S groups of sac, respectively. The well-resolved signals at 30.9–28.0 ppm were assigned to the CH_2 group of PPh_2Bz. In the ^{31}P NMR spectra of **1**–**4**, the signals of free PPh_2Py (−5.5 ppm) and PPh_2Bz (−10.4 ppm) ligands experienced significant deshielding upon coordination to Pd(II) and Pt(II) metal ions. The spectra of Pd(II) complexes (**1** and **3**) presented a singlet at 23.5 and 54.5 ppm, respectively. On the other hand, the presence of two doublets in the spectra of **2** confirmed non-equivalent P nuclei of two PPh_2Py ligands in the *cis* position with a $^2J_{PP}$ coupling constant of 12.9 Hz. In addition, the ^{31}P ^{195}Pt coupling in **2** resulted in a set of characteristic satellite lines with an intensity of ∼1:4:1, yielding two $^1J_{PtP}$ coupling constants of 3457 and 3635 Hz. A singlet corresponding to a P nucleus was observed in the spectra of **4** ($^2J_{PP}$ = 14.9 Hz and $^1J_{PtP}$ = 2219 Hz) indicating the *trans* configuration of two PPh_2Bz ligands. The $^1J_{PtP}$ constants correlate well with those reported for *cis* and *trans* isomers of Pt(II) complexes with chlorido and monophosphines.[24,33,34]

The species generated under the experimental conditions of the positive ion electrospray ionization mass spectroscopy (ESI-MS) measurements of **1**–**4** are shown in Figure S3. The molecular ion peaks in the ESI-MS spectra correspond to $[M - sac]^+$ for **1** and **3**, due to loss of sac, while *m*/*z* 904.0 and 988.1 in the spectra of **2** and **4** are consistent with $[M - Cl]^+$ and $[M + Na]^+$, respectively. The base peaks in the spectra of **1**, **3** and **4** are related to $[M(Phos)_2 - H]^+$, except for an inclusion of MeOH to **1**. The highest signal at *m*/*z* 756.9 in the spectra of **2** correlates well with $[M - sac]^+$.

2.2 | X-ray structures

Slow evaporation of the solutions of **1**–**4** in a dimethylformadide (DMF)/ethanol (EtOH) mixture provided single crystals suitable for single-crystal X-ray diffraction (XRD). However, the crystals of **1** did not produce diffraction. The crystallographic data and the parameters of refinement process for **2**–**4** are summarized in Table S1, while the selected bond distances and angles are listed in Table 1. As shown in Table 1 and Figure 1, all the complexes display a distorted square planar geometry due to the steric bulk of the phosphine and sac ligands. The Pd(II) complex (**3**) has two phosphines and two sac ligands at the *cis* positions. The Pt(II) complexes (**2** and **4**) consist of a chlorido, a sac and two phosphine ligands. In **2**, the sac ligand is *cis* to the chlorido ligand,

TABLE 1 Selected bond distances (Å) and angles (°) for **2**–**4**.

	2	3	4
M1—N1	2.070(7)	2.083(5)	2.023(7)
M1—N2	-	2.091(5)	-
M1—P1	2.239(2)	2.291(2)	2.319(3)
M1—P2	2.259(2)	2.302(2)	2.299(3)
M1—Cl1	2.335(2)	-	2.296(3)
N1—M1—N2	-	86.39(19)	-
N1—M1—P1	91.18(19)	89.28(13)	92.2(2)
N1—M1—P2	169.33(19)	175.82(14)	92.2(2)
N2—M1—P1	-	175.32(15)	-
N2—M1—P2	-	90.35(14)	-
P1—M1—P2	97.21(8)	94.05(5)	173.05(9)
N1—M1—Cl1	86.51(19)	-	175.55(19)
P1—M1—Cl1	176.23(8)	-	88.86(9)
P2—M1—Cl1	85.43(8)	-	87.16(9)

10990739, 0, Downloaded from https://onlinelibrary.wiley.com/doi/10.1002/aoc.7433 by Dokuz Eylul University, Wiley Online Library on [06/03/2024]. See the Terms and Conditions (https://onlinelibrary.wiley.com/terms-and-conditions) on Wiley Online Library for rules of use; OA articles are governed by the applicable Creative Commons License

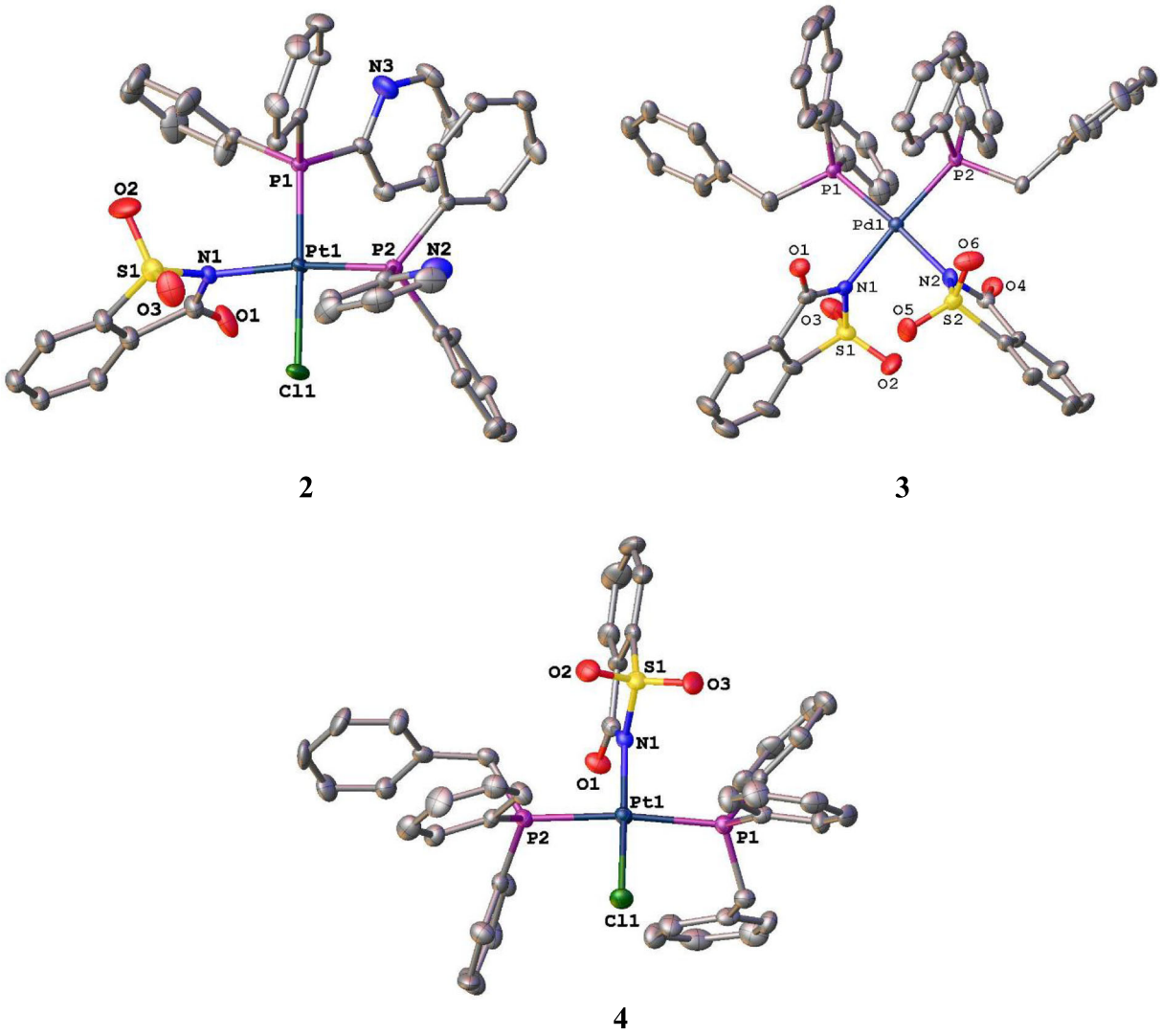

FIGURE 1 Molecular structures of **2**–**4** with thermal ellipsoids at 40% probability. CH hydrogens were omitted for clarity. The disordered DMF molecules in **2** and **3** were not shown.

but it is *trans* to chlorido in **4**. The Pd—N and Pd—P bond distances in **3** are similar to those in *cis*-[Pd(sac)$_2$(ter-phos)$_2$],[35] and *cis*-[PdCl$_2$(PPh$_2$Bz)$_2$].[36] The Pt—P bond distances in **4** are remarkably bigger than those in **2**, correlating with the cone angles of PPh$_2$Py and PPh$_2$Bz (145° and 152°, respectively).[37] On the other hand, the Pt—Cl and Pt—N bond distances in **2** are markedly longer than the same bonds in **4**, indicating the greater *trans* effect of PPh$_2$Py compared with both sac and chlorido ligands. The Pt—N, Pt—P and Pt—Cl bond distances in **2** and **4** compare well with those reported in *cis*- or *trans*-[PtCl(sac)(ter-phos)$_2$],[22–28] In the crystalline state, the molecules of **2**–**4** are packed into a hydrogen-bonded three-dimensional network by a number of weak intermolecular C—H···O hydrogen bonds. The C—H···Cl contacts further reinforce the packing interactions in **2** and **4**.

2.3 | Cytotoxic activity of the complexes

Complexes **1**–**4** and free ligands were tested for in vitro cytotoxicity against a panel of seven cancer cell lines including HCT116, HepG2, MDA-MB-231, PANC-1, A549, C6, DU145 and BEAS-2B as cell line. The viability was measured by sulforhodamine B (SRB) cell viability assay after treatment with different concentrations (0.63–40 μM) of the complexes, ligands and cisplatin. The dose–response curves presented in Figure S4 were used to calculate the IC$_{50}$ values (Table 2).

The results showed that the free ligands, Na(sac), PPh$_2$Py and PPh$_2$Bz were not cytotoxic below 40 μM against all the cell lines. Similarly, complexes **1** and **2** did not practically show biological activity, with the exception of **1**, which displayed a lower cell growth inhibition towards MDA-MB-231 and C6 cells. However, **3** and

10990739, 0, Downloaded from https://onlinelibrary.wiley.com/doi/10.1002/aoc.7433 by Dokuz Eylul University, Wiley Online Library on [06/03/2024]. See the Terms and Conditions (https://onlinelibrary.wiley.com/terms-and-conditions) on Wiley Online Library for rules of use; OA articles are governed by the applicable Creative Commons License

TABLE 2 Cytotoxic activity (IC_{50}, μM) of complexes **1**–**4**, cisplatin and the ligands against different cells after 48 h of treatment.

	HCT116	HepG2	MDA-MB-231	PANC1	A549	C6	DU145	BEAS-2B
1	>40	>40	24.0 ± 0.8	>40	>40	27.9 ± 0.2	>40	23.8 ± 0.5
2	>40	>40	>40	>40	>40	>40	>40	>40
3	7.0 ± 1.0	32.4 ± 1.0	6.2 ± 0.1	15.3 ± 1.2	>40	4.9 ± 0.2	35.2 ± 0.5	4.9 ± 1.8
4	4.3 ± 0.7	7.3 ± 0.4	5.3 ± 1.9	12.1 ± 0.4	7.1 ± 1.0	2.2 ± 0.1	6.5 ± 1.4	7.7 ± 1.2
Cisplatin	18.5 ± 0.3	15.4 ± 2.9	37.7 ± 2.0	>40	14.7 ± 1.1	15.4 ± 3.2	32.9 ± 1.7	7.6 ± 0.4
Na(sac)	>40	>40	>40	>40	>40	>40	>40	>40
PPh_2Py	>40	>40	>40	>40	>40	>40	>40	>40
PPh_2Bz	>40	>40	>40	>40	>40	>40	>40	>40

Note: HCT116 (colon), HepG2 (liver), MDA-MB-231 (breast), PANC-1 (pancreatic), A549 (lung), C6 (glioma), DU145 (prostate) cancer cells and BEAS-2B (normal human lung epithelial cells). IC_{50} values are presented as the mean ± SD (standard deviation) from three independent experiments.

4 decreased the cell viability in a dose dependent manner. It was remarkable that the lowest IC_{50} values were observed for the *trans*-configured complex **4** among all complexes, exhibiting an extremely higher cytotoxic potency than **3** and cisplatin. In addition, the cytotoxicity of the complex on cancerous cells was much more than normal cells. As complex **4** demonstrated the most potent cytotoxicity against HCT116 and C6 cell lines, further studies were continued with HCT116 cells, owing to the rat origin of C6 cells.

2.4 | Hydrolysis and stability of the potent complexes

The square planar complexes of Pd(II) and Pt(II) undergo ligand substitution reactions, and Pd(II) complexes display 10^{-3}–10^{-5} higher reactivity than their Pt(II) analogues.[38] The time-dependent hydrolysis of the most potent complexes (**3** and **4**) was investigated in a physiological solution (saline, an aqueous solution of 0.9% NaCl containing 0.2% dimethyl sulfoxide [DMSO]) by UV–vis spectroscopy at 298 K. The position and intensity of absorption bands in the spectra of both complexes remained unchanged up to 4 h (Figure S5). The results suggested that the complexes are not involved in the ligand exchange reaction.

The solution stability of **3** and **4** in saline was screened by using UV–vis spectra measured up to 48 h. As shown in Figure S5, no notable change was observed in the spectra of both complexes. In addition, the stability of the complexes is also assessed in neat DMSO using NMR spectroscopy. It was observed that the ^{31}P NMR spectra of these complexes at 0, 24 and 48 h were identical, indicating the solution stability of both complexes in DMSO (Figure S6).

2.5 | Cellular uptake and lipophilicity

The different biological activities of **1**–**4** may be attributed to the structural differences in the complexes and the characteristics of the ligands. If the isomerization is ignored, complexes **2** and **4** are structurally similar but contain PPh_2Py and PPh_2Bz ligands, respectively. To better understand the higher cytotoxic activity of **4**, and the ineffectiveness of **2**, cellular uptake studies were performed. After the treatment of HCT116 cells with **2**, **4** and cisplatin (10 μM) for 12 h, the accumulation of Pt in HCT116 cells was quantified using an ICP-OES spectrometer as pmol Pt(II) complex per million cells. Cisplatin was highly accumulated in HCT116 cells (664.4 ± 31.9 pmol/10^6 cells), and **4** was also effectively taken up by cells (510.6 ± 23.0 pmol/10^6 cells), whereas **2** showed much lower uptake, with an amount of (20.6 ± 1.8 pmol/10^6 cells). Significantly higher cellular uptake of **4** is in accord with its stronger cytotoxic activity.

The differentiation of the cytotoxicity and cellular uptake of **2** and **4** may be related to the lipophilicity of the complexes. The partition coefficient log*P* is frequently used to evaluate the lipophilicity of a compound[39,40] and considered as an important parameter for the accumulation of Pt complexes into cells.[41,42] Cisplatin is hydrophilic, with a negative clog*P* value of −2.50. The presence of large nonpolar PPh_2Py and PPh_2Bz ligands substantially increased the lipophilicity of **2** (clog*P* = 9.78) and **4** (clog*P* = 13.45). Obviously, the Py ring remarkably enhances the hydrophilicity of PPh_2Py, while the benzyl group increases the hydrophobicity of PPh_2Bz. The Py groups in the PPh_2Py ligands in **1** and **2** seem to retard the crossing of these complexes the cell membrane. As a result, complexes **3** and **4** bearing two PPh_2Bz ligands exhibit much higher diffusion ability into the cells and stronger cytotoxic activity in comparison with **1** and **2**.

10990739, 0, Downloaded from https://onlinelibrary.wiley.com/doi/10.1002/aoc.7433 by Dokuz Eylul University, Wiley Online Library on [06/03/2024]. See the Terms and Conditions (https://onlinelibrary.wiley.com/terms-and-conditions) on Wiley Online Library for rules of use; OA articles are governed by the applicable Creative Commons License

2.6 | Structure–activity relationship

It is very important to explain the structure–activity relationships of the present complexes because their structures and properties significantly affect their biological activity. The present complexes and ligands were evaluated for their cytotoxic properties. It was shown that the complexes presented improved cytotoxic activities with respect to the parent sac and phosphine ligands a result of overall chemical–physical properties of the resulting complex. It is well known that the administration of drugs is mainly determined by their lipophilicity and stability in plasma. Although Pd(II) complexes are known to be kinetically unstable compared with their Pt(II) counterparts, the hydrolysis and stability studies demonstrated that **3** and **4** did not undergo ligand exchange reactions in saline and DMSO, indicating their structural stability in various solutions. On the other hand, the lipophilicity is a balance between hydrophilicity and hydrophobicity, being conditioned by the nature of the ligands in metal complexes. Moreover, the lipophilicity increases the diffusion of molecules across the cell membrane. It was observed that the lipophilicity of the present complexes mainly depends on the incorporation of Py and Bz groups onto the phosphine ligands. The presence of the Bz group increases the lipophilicity of complexes **3** and **4** and favours their cellular uptake in comparison with **1** and **2**. As a result, both **3** and **4** display potent cytotoxicity against cancer cells, **4** being more prominent than **3**. In addition, the stereochemistry around Pt(II) is known to change the chemical reactivity and in turn anticancer properties of Pt(II) complexes. The clinically used platinum drugs have a *cis*-configuration, but it has been well documented that some *trans* platinum complexes showed better anticancer activities than cisplatin.[43–46] The most potent complex (**4**) has a *trans*-configured structure and is an interesting example of nonclassical platinum(II) complexes.

2.7 | Evaluation of cell death

HCT116 cells were incubated for 12 and 24 h with IC_{75} doses of **4** (20 μM) and cisplatin (40 μM) and analysed by flow cytometry.

2.7.1 | Cell apoptosis

In early apoptotic cells, phosphatidylserine moves to the extracellular surface and can be detected with annexin V coupled to a fluorescent dye such as 7-aminoactinomycin D (7-AAD) by flow cytometry.[47] The percentages of HCT116 cells undergoing early and late apoptosis after 12 and 24 h exposure are illustrated in Figures 2a and S7. The data obtained at 24 h reveal that **4** induced apoptosis in HCT116 cells by 58.4% (early, 7.5; late, 50.9%), being much higher than 50% (early, 12.9; late, 37.1%) recorded for cisplatin.

Executioner caspases (3 and 7) are activated during apoptosis, ultimately causing cellular death through cleavage of cellular proteins.[48] The observations obtained by the annexin V assay were further supported by caspase 3/7 activity, which revealed abundant caspase (+)/7-AAD (+) cells (apoptotic/dead). A time-dependent increase in the caspase 3/7 activation is shown in HCT116 cells treated with **4** so that 66.9% of cells were apoptotic (8.1%) and apoptotic/dead (58.8%) at 24 h (Figures 2b and S8). On the other hand, the percentage of early and late apoptotic cells was 55.2% after 24 h of treatment with cisplatin. Thus, it is clear that **4** can induce cell death through the apoptotic pathway.

The apoptotic cell death mechanism can be followed by inhibition of the antiapoptotic Bcl-2 proteins, which regulate mitochondria-mediated apoptosis.[49] The Ser-70 phosphorylation of Bcl-2 was examined by flow cytometry. The treatment with **4** increased the phosphorylation of Bcl-2 in HCT116 cells in a time-dependent manner (Figures 2c and S9). The inactivated Bcl-2 expression in untreated HCT116 cells (control) is 7.9%, and the phosphorylation of Bcl-2 increased to 34.2% and 55.6% after exposure to **4** for 12 and 24 h, respectively. The Bcl-2 expressions were remarkably low in the case of cisplatin. These findings approve the strong inhibition of Bcl-2 by **4** in HCT 116 cells and thereby induction of apoptotic cell death through the mitochondrial pathway.

2.7.2 | Intracellular ROS generation

ROS are mostly generated by mitochondria as by-products and play important roles in various biological processes. Metal complexes are capable of regulation of the ROS levels in cancer cells to damage mitochondria and DNA, ultimately inducing cancer cell death.[50] Elevating of ROS levels of cancer cells may be an appealing approach for cancer chemotherapy. We have shown earlier that Pt(II) sac complexes with phosphine ligands increased the generation of ROS and induced apoptosis via the oxidative stress pathway.[23–28] As shown in Figures 3a and S10, the amount of the oxidatively stressed HCT116 cells was greatly increased with exposure to **4**, due to the elevated levels of ROS. However, the effect of ROS was found much higher in the cells treated with cisplatin.

10990739, 0, Downloaded from https://onlinelibrary.wiley.com/doi/10.1002/aoc.7433 by Dokuz Eylul University, Wiley Online Library on [06/03/2024]. See the Terms and Conditions (https://onlinelibrary.wiley.com/terms-and-conditions) on Wiley Online Library for rules of use; OA articles are governed by the applicable Creative Commons License

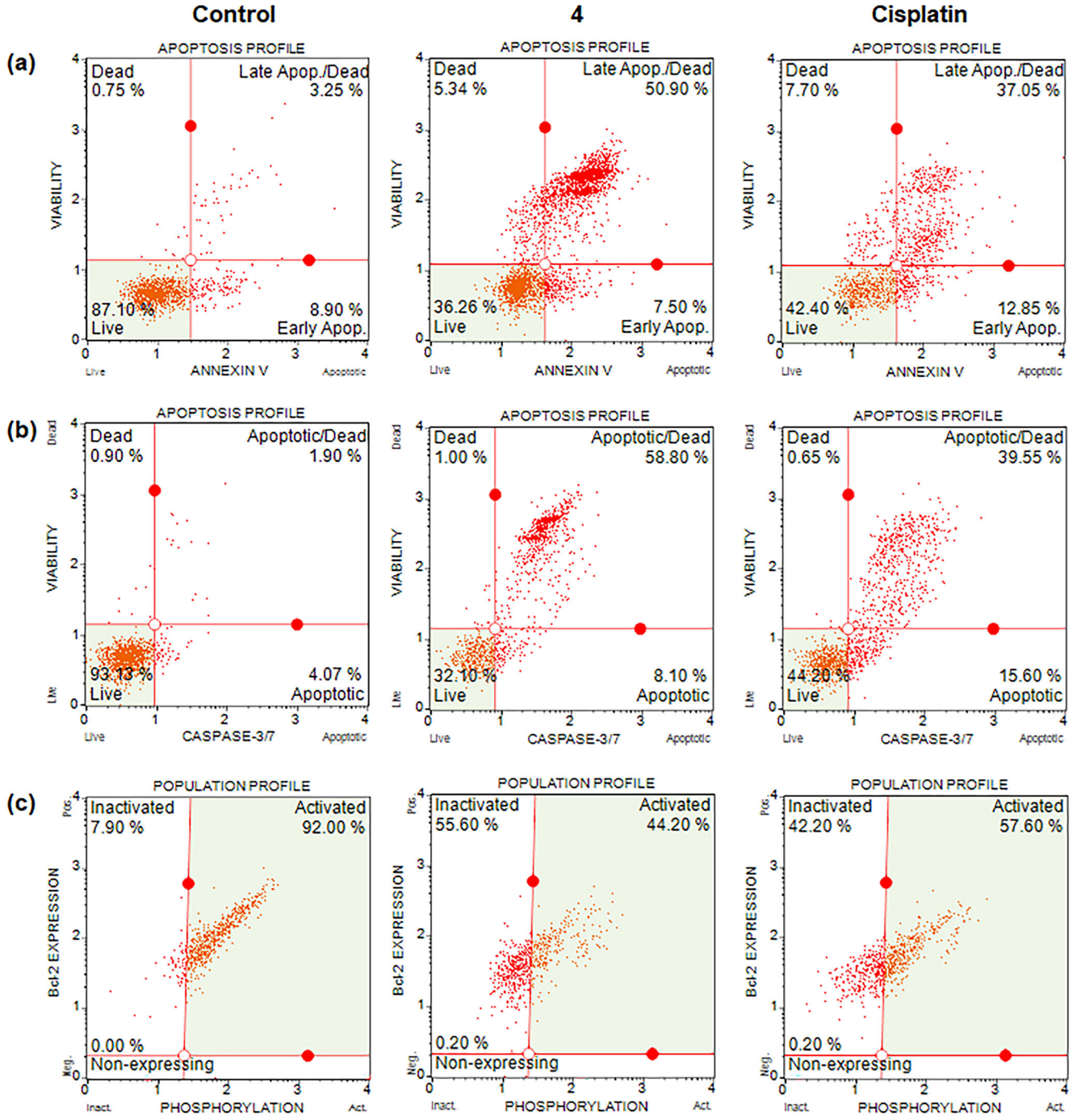

FIGURE 2 Detection of apoptosis in HCT116 cells after 24 h of treatment with the IC_{75} concentrations of **4** (20 μM) and cisplatin (40 μM), using (a) annexin V, (b) caspase 3/7 and (c) Bcl-2 assays.

2.7.3 | DNA damage

DNA is the main target of metal complexes and cytotoxic agents usually damage genomic DNA, especially in the form of DSBs. Moreover, an excessive amount of intracellular ROS can cause DSBs in cells.[51] The presence of DSBs is detected and quantified by flow cytometry due to the formation of the Ser-139 phosphorylated γ-H2AX in response to DNA damage.[52,53] The treatment with **4** and cisplatin resulted in a time-dependent increase in the DSBs levels in HCT116 cells (indicated as activated) (Figures 3b and S11). At 12 h, cisplatin produced higher phosphorylation, but the DSBs levels of **4** and cisplatin were comparable at 24 h. These findings strongly imply

10990739, 0, Downloaded from https://onlinelibrary.wiley.com/doi/10.1002/aoc.7433 by Dokuz Eylul University, Wiley Online Library on [06/03/2024]. See the Terms and Conditions (https://onlinelibrary.wiley.com/terms-and-conditions) on Wiley Online Library for rules of use; OA articles are governed by the applicable Creative Commons License

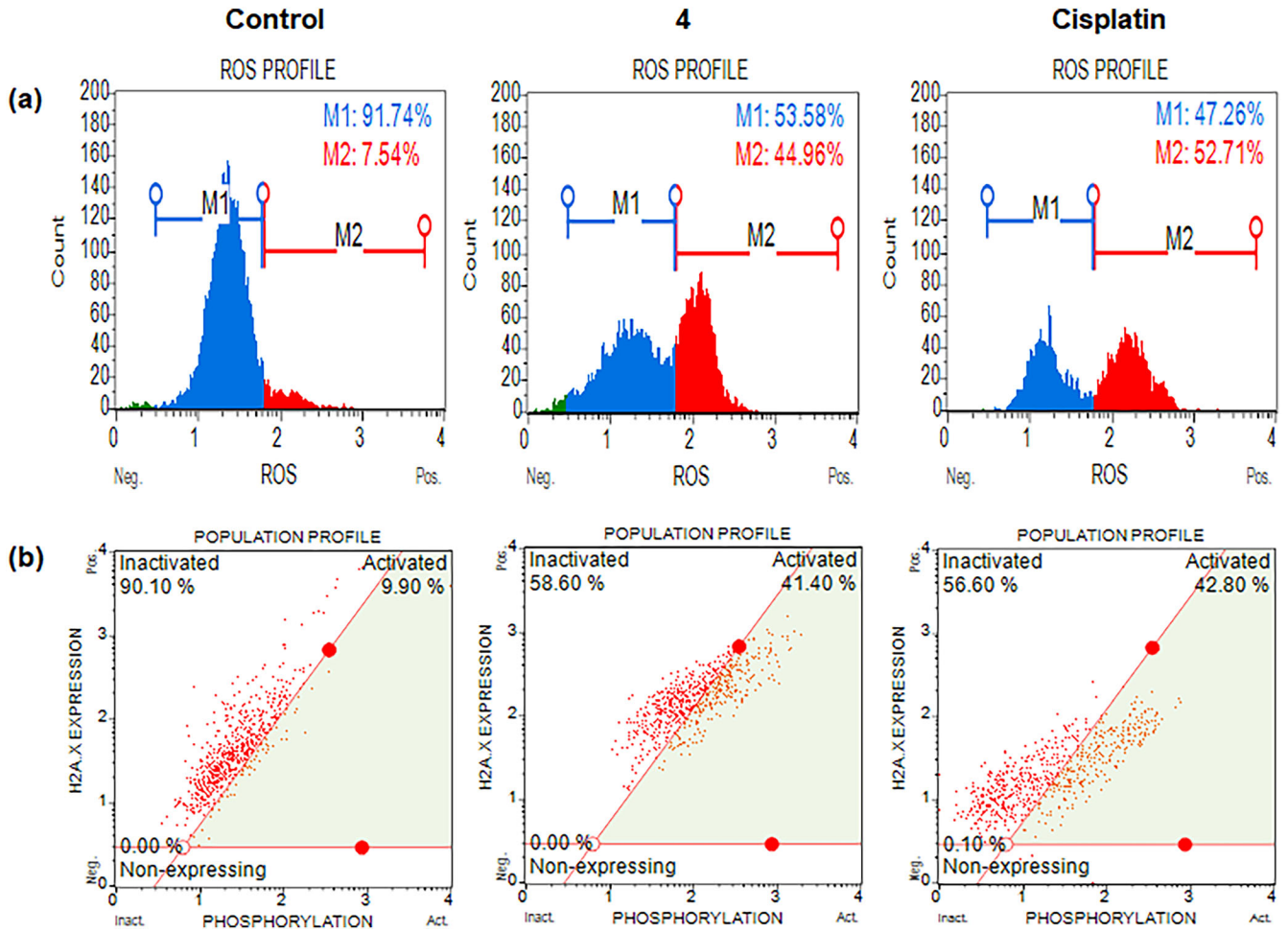

FIGURE 3 (a) Oxidative stress and (b) DNA damage induced in HCT116 cells after 24 h of exposure to the IC_{75} concentrations of **4** (20 μM) and cisplatin (40 μM).

that the observed DNA damage may be related to the elevation of intercellular ROS caused by **4**.

2.8 | Antiangiogenic activity

The chick chorioallantoic membrane (CAM) assay is widely used to study angiogenesis.[54] CAM is an extraembryonic membrane, forming an intensive capillary network to observe angiogenesis in vivo. In addition, it enables the investigation of tumour formation and metastasis.[55] The modulation of the process of angiogenesis by transition metals and their complexes is comprehensively reviewed recently by Dürig et al.[56] Our previous studies have demonstrated that several Pd(II) sac complexes displayed promising antiangiogenic activity.[57,58]

The antiangionetic potential of **4** was investigated via the CAM assay. In principle, relatively lower doses are preferential for the evaluation of antiangiogenic effects of any compound. Therefore, remarkably low doses were used to evaluate the antiangiogenic potential of **4**, and the results were compared with those of a well-known antiangiogenic drug thalidomide.[59,60] As shown in Figure 4, the dose of 50 ng per egg showed strong antiangiogenic effect after 24 h of treatment. The Pt(II) complex significantly inhibited formation and branching of new blood vessels compared with the control, revealing its promising antimetastatic potential. The average antiangiogenic score of **4** was estimated as 1.3 ± 0.4 using the method reported by Krenn and Paper.[61] The score was higher than those reported for Pd(II) complexes bearing sac with a dose of 50 μg per egg[57,58] but somewhat lower than that of the positive control thalidomide at a dose of 50 μg (1.5 ± 0.5).

In fact, higher doses (100 and 200 ng per egg) of **4** were also used in the experiments, but they displayed strong toxicity, preventing us from drawing reliable conclusion about its impact on angiogenesis (data not

10990739, 0, Downloaded from https://onlinelibrary.wiley.com/doi/10.1002/aoc.7433 by Dokuz Eylul University, Wiley Online Library on [06/03/2024]. See the Terms and Conditions (https://onlinelibrary.wiley.com/terms-and-conditions) on Wiley Online Library for rules of use; OA articles are governed by the applicable Creative Commons License

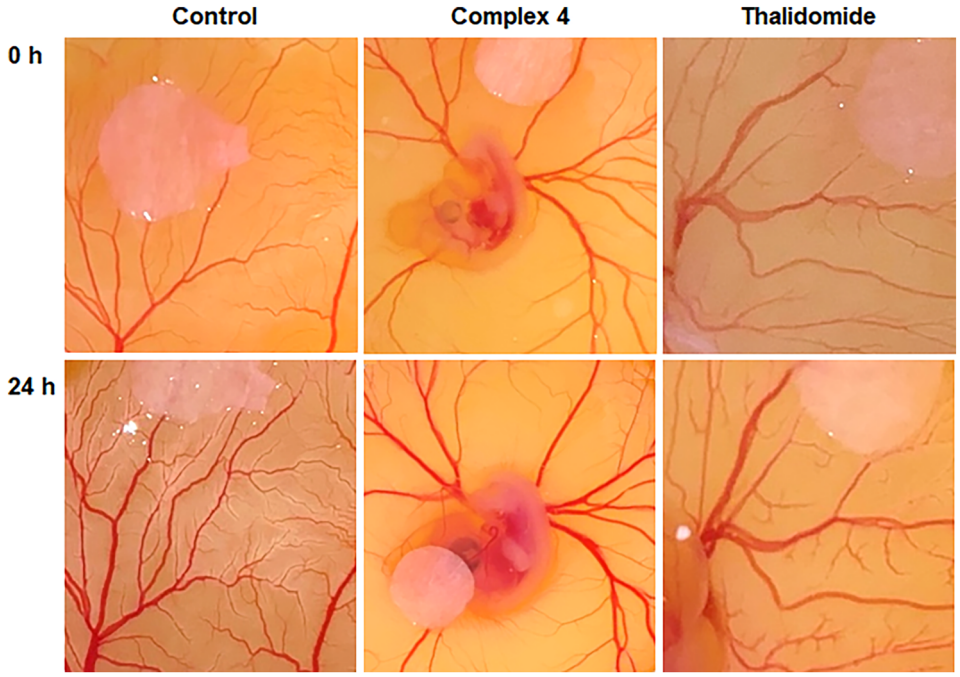

FIGURE 4 Effect of **4** on angiogenesis after 24 h of treatment in a chick embryo CAM model. **4** and thalidomide (the positive control) were used as 50 ng and 50 μg per egg, respectively.

shown). Despite these promising findings, the present study was limited to in ovo model, and further studies are required to confirm these observations in in vivo mammalian models.

3 | CONCLUSIONS

In summary, four novel Pd(II) and Pt(II) sac complexes of PPh_2Py and PPh_2Bz have been synthesized and structurally characterized. The complexes bearing PPh_2Py seemed to be practically non-cytotoxic at the concentration range tested, while the complexes with PPh_2Bz displayed significant cytotoxicity against cancer cell lines. The difference in the potency of the complexes was associated to their cellular uptake. Especially *trans*-[PtCl(sac)$(PPh_2Bz)_2$] (**4**) showed increased potency with respect to cisplatin. In addition, this complex mostly produced higher selectivity towards cancer cells than normal cells. The results indicated **4** as a highly potent complex in HCT116 cells, to be further involved in the evaluation of cell death mechanism studies. The results demonstrated that **4** induced apoptosis due to inhibition of Bcl-2 proteins, generation of intracellular oxidative stress, leading to DNA damage. Furthermore, the study revealed the strong angiogenesis inhibitory action of **4** as evidenced by the in ovo CAM model. Finally, **4** showed potent anticancer and antiangiogenic activities and may therefore be recommended as a promising multi-targeted agent for antiangiogenic cancer treatment. Furthermore, the complex could be a potential candidate for further studies to develop a new *trans*-configured Pt(II) antitumor drug due to its attractive biological performance.

4 | EXPERIMENTAL

4.1 | Materials and measurements

[PtCl(sac)(COD)] was synthesized by following the method as previously reported by Icsel.[31] All other reagents were obtained commercially and used as received. Elemental analyses (C, H and N) were performed using a Costech elemental analyser. UV–vis and IR spectra were measured on a Perkin Elmer Lambda 35 and a Perkin Elmer Spectrum Two FT-IR spectrophotometer, respectively. NMR spectra were recorded using a Bruker Avance Neo 500 MHz spectrometer in DMSO-d_6. The ESI-MS spectra were carried out on a Waters Alliance HPLC and ZQ micromass LS-MS spectrometer. The solution conductivity measurements were performed using HANNA HI 5521.

4.2 | Synthesis of Pd(II) and Pt(II) complexes

Pd(II) complexes (**1** and **3**) were synthesized by following the general procedure. The solid sacH (92 mg, 0.50 mmol) was directly added to a solution of $Pd(OAc)_2$ (56 mg, 0.25 mmol) in MeCN (15 mL) with stirring. Ten millilitres of water was then added to the solution and

10990739, 0, Downloaded from https://onlinelibrary.wiley.com/doi/10.1002/aoc.7433 by Dokuz Eylul University, Wiley Online Library on [06/03/2024]. See the Terms and Conditions (https://onlinelibrary.wiley.com/terms-and-conditions) on Wiley Online Library for rules of use; OA articles are governed by the applicable Creative Commons License

stirred at rt. The addition of PPh_2Py and PPh_2Bz (0.50 mmol) in 10 mL of a MeOH and chloroform mixture (1:1, v:v) to the reaction mixture resulted in clear pale yellow solutions. The solutions were then stirred for 24 h at rt, and the solvent was then removed, using a rotary evaporator. The powders of the complexes were dissolved in a DMF/EtOH mixture (1:1, v:v), and the slow evaporation of these solutions provided yellowish crystals suited to single-crystal XRD within 10 days.

Pt(II) complexes (**2** and **4**) were obtained by the reaction of [PtCl(sac)(COD)] (65 mg, 0.25 mmol) in MeCN (50 mL) with PPh_2Py and PPh_2Bz (0.50 mmol) in MeCN after stirring 6 h at 65°C. The solvent was removed, using a rotary evaporator. The crystallization of both complexes in a DMF/EtOH (1:1, v:v) solution yielded X-ray quality colourless crystals after 2 months. The yields, elemental analysis and characterization data referred to the crystalline complexes.

4.2.1 | *cis*-[Pd(sac)$_2$(PPh2Py)$_2$] (1)

Yellow powder. Yield: 219 mg (88%). Anal. Calcd for $C_{48}H_{36}N_4O_6P_2PdS_2$ (%): C, 57.81; H, 3.64; N, 5.62. Found C, 57.98; H, 3.80; N, 5.40. IR (ν/cm^{-1}): 3054w, 2914vw, 2855vw, 1675w, 1654s (CO), 1585m, 1484w, 1456m, 1434m (CC), 1328w $(CNS)_{sym}$, 1294s, 1283s, 1248m $(SO_2)_{asym}$, 1152s $(SO_2)_{sym}$, 1095m, 1055m, 1015w $(PC)_{sym}$, 955s $(CNS)_{asym}$, 850w, 781m, 748s, 678s, 644m, 595s, 530vs, 498vs $(PC)_{asym}$. ^{1}H NMR (400.13 MHz, DMSO-d_6, δ, ppm): 8.86–8.69 (d, 2H, H6′-Py, $J_{HH} = 4.0$ Hz), 8.66–8.56 (tt, 2H, H3′-Py, $J_{HH} = 4.0$ Hz, $J_{HH} = 4.0$ Hz), 8.48–8.21 (d, 2H, H4′-Py, $J_{HH} = 4.0$ Hz), 8.18–6.60 (m, 2H, H5′-Py, 20H-Ph, 8H-sac). ^{13}C{^{1}H} NMR (100.62 MHz, DMSO-d_6, δ, ppm): 165.2 (s, C_7-sac), 159.2 (s, $C_{2'}$), 149.7 (d, $C_{6'}$, $J_{PC} = 16.1$ Hz), 142.4 (s, C_1-sac), 135.0 (s, $C_{ipso\text{-}Ph}$), 133.4 (d, $C_{4'}$, $J_{PC} = 11.1$ Hz), 132.4 (s, C_3-sac), 131.9 (d, $C_{ortho\text{-}Ph}$, $J_{PC} = 12.1$ Hz), 131.4 (s, C_6-sac), 130.9 (s, $C_{3'}$), 130.3 (d, $C_{meta\text{-}Ph}$, $J_{PC} = 9.1$ Hz), 128.0 (s, C_4-sac), 127.8 (s, $C_{para\text{-}Ph}$), 127.1 (s, $C_{5'}$), 122.6 (s, C_5-sac), 119.1 (s, C_2-sac). ^{31}P{^{1}H} NMR (161.97 MHz, DMSO-d_6, δ, ppm): δ (ppm) 23.5 (s). Molar conductivity, Λ_M (MeOH, 298 K, 1 mM) 11.3 S cm^2 mol^{-1} (nonelectrolyte). ESI-MS (m/z, MeOH): 814.8 (9%, calcd 815.1) $[M - sac]^+$, 665.4 (100%, calcd 665.0) $[Pd(PPh_2Py)_2(MeOH) - H]^+$.

4.2.2 | *cis*-[PtCl(sac)(PPh_2Py)$_2$]·0.5DMF (2)

Colourless crystals. Yield: 212 mg (87%). Anal. Calcd for $C_{42.5}H_{35.5}ClN_{3.5}O_{3.5}P_2PtS$ (%): C, 52.31; H, 3.67; N, 5.02. Found C, 52.59; H, 3.52; N, 5.25. IR (ν/cm^{-1}): 3066w, 2856vw, 1675s (CO), 1592w, 1572m, 1483m, 1435s (CC), 1421m, 1306s $(CNS)_{sym}$, 1276s, 1250s $(SO_2)_{asym}$, 1172s, 1155s $(SO_2)_{sym}$, 1093s, 988m $(PC)_{sym}$, 953s $(CNS)_{asym}$, 783m, 742s, 694s, 674s, 591s, 555s, 532vs, 525vs, 511vs $(PC)_{asym}$, 482vs, 454m. ^{1}H NMR (400.13 MHz, DMSO-d_6, δ, ppm): 9.05–8.71 (d, 2H, H6′-Py, $J_{HH} = 4.0$ Hz), 8.66–8.32 (tt, 2H, H3′-Py, $J_{HH} = 4.0$ Hz, $J_{HH} = 4.0$ Hz), 8.27–6.95 (m, 4H, H4′, 5′-Py, 20H-Ph, 4H-sac). ^{13}C{^{1}H} NMR (100.62 MHz, DMSO-d_6, δ, ppm): 164.4 (s, C_7-sac), 157.5 (s, $C_{2'}$), 150.6 (d, $C_{6'}$, $J_{PC} = 13.1$ Hz), 141.5 (s, C_1-sac), 132.5 (d, $C_{4'}$, $J_{PC} = 11.2$ Hz), 131.7 (s, $C_{ipso\text{-}Ph}$), 130.9 (s, C_3-sac), 130.5 (s, $C_{3'}$), 130.1 (d, $C_{ortho\text{-}Ph}$, $J_{PC} = 6.1$ Hz), 129.8 (s, C_6-sac), 127.8 (d, $C_{meta\text{-}Ph}$, $J_{PC} = 11.1$ Hz), 125.7 (s, C_4-sac), 124.6 (s, $C_{para\text{-}Ph}$), 124.1 (s, $C_{5'}$), 119.5 (s, C_5-sac), 119.0 (s, C_2-sac). ^{31}P{^{1}H} NMR (161.97 MHz, DMSO-d_6, δ, ppm): 39.1 (d, ^1JPtP$_a$ = 3456.9 Hz, ^2JP$_a$P$_b$ = 12.9 Hz), 18.7 (d, ^1JPtP$_b$ = 3634.8 Hz, ^2JP$_b$P$_a$ = 12.9 Hz). Molar conductivity, Λ_M (MeOH, 298 K, 1 mM) 8.3 S cm^2 mol^{-1} (nonelectrolyte). ESI-MS (m/z, MeOH): 904.0 (5%, calcd 903.8) $[M - Cl]^+$, 756.9 (100%, calcd 757.1) $[M - sac]^+$.

4.2.3 | *cis*-[Pd(sac)$_2$(PPh_2Bz)$_2$]·DMF (3)

Yellow crystals. Yield: 203 mg (74%). Anal. Calcd for $C_{55}H_{49}N_3O_7P_2PdS_2$ (%): C, 60.25; H, 4.50; N, 3.83. Found C, 60.13; H, 4.65; N, 3.67. IR (ν/cm^{-1}): 3077w, 2919w, 2856w, 1678m, 1658s (CO), 1591m, 1495m, 1458m, 1435m (CC), 1386m, 1330m $(CNS)_{sym}$, 1296s, 1285s, 1245s $(SO_2)_{asym}$, 1154s $(SO_2)_{sym}$, 1101s, 1059m, 1013m $(PC)_{sym}$, 968s $(CNS)_{asym}$, 846m, 779m, 757s, 741s, 678s, 596vs, 585s, 536m, 523m, 499vs $(PC)_{asym}$, 455m. ^{1}H NMR (400.13 MHz, DMSO-d_6, δ, ppm): 8.22–6.50 (m, 30H-Ph, 8H-sac), 4.10–3.93 (d, 4H, CH_2-benzyl, $^2J_{HP} = 12.0$ Hz). ^{13}C{^{1}H} NMR (100.62 MHz, DMSO-d_6, δ, ppm): 164.3 (s, C_7-sac), 145.8 (s, C_1-sac), 134.5 (s, $C_{para\text{-}Bz}$), 134.3 (d, $C_{ipso\text{-}Bz}$, $J_{PC} = 24.1$ Hz), 133.4 (s, $C_{ipso\text{-}Ph}$), 132.8 (d, $C_{meta\text{-}Ph}$, $J_{PC} = 10.1$ Hz), 129.9 (d, $C_{ortho\text{-}Ph}$, $J_{PC} = 11.1$ Hz), 129.6 (s, $C_{para\text{-}Ph}$), 128.9 (s, C_3-sac), 128.2 (d, $C_{ortho\text{-}Bz}$, $J_{PC} = 7.0$ Hz), 127.4 (s, C_6-sac), 127.0 (d, $C_{meta\text{-}Bz}$, $J_{PC} = 11.1$ Hz), 126.7 (s, C_4-sac), 123.7 (s, C_5-sac), 120.3 (s, C_2-sac), 26.9 (s, CH_2-Bz). ^{31}P{^{1}H} NMR (161.97 MHz, DMSO-d_6, δ, ppm): δ (ppm) 54.5 (s). Molar conductivity, Λ_M (MeOH, 298 K, 1 mM) 10.8 S cm^2 mol^{-1} (nonelectrolyte). ESI-MS (m/z, MeOH): 841.0 (9%, calcd 841.2) $[M - sac]^+$, 657.8 (100%, calcd 658.0) $[Pd(PPh_2Bz)_2 - H]^+$, 383.5 (38%, calcd 383.0) $[Pd(PPh_2Bz) - H]^+$.

4.2.4 | *trans*-[PtCl(sac)(PPh_2Bz)$_2$] (4)

Colourless crystals. Yield: 191 mg (79%). Anal. Calcd for $C_{45}H_{38}ClNO_3P_2PtS$ (%): C, 55.99; H, 3.97; N, 1.45.

10990739, 0, Downloaded from https://onlinelibrary.wiley.com/doi/10.1002/aoc.7433 by Dokuz Eylul University, Wiley Online Library on [06/03/2024]. See the Terms and Conditions (https://onlinelibrary.wiley.com/terms-and-conditions) on Wiley Online Library for rules of use; OA articles are governed by the applicable Creative Commons License

Found C, 55.84; H, 4.13; N, 1.51. IR (ν/cm^{-1}): 3066vw, 3030vw, 2917w, 2850w, 1667m (CO), 1589w, 1494w, 1453w, 1438m (CC), 1336w $(CNS)_{sym}$, 1304s, 1292s, 1252m $(SO_2)_{asym}$, 1228w, 1170m, 1154s $(SO_2)_{sym}$, 1104s, 1068m, 1030m, 997w $(PC)_{sym}$, 967m $(CNS)_{asym}$, 911w, 833m, 773s, 743s, 698vs, 680s, 596s, 584s, 563s, 538m, 519m, 496vs $(PC)_{asym}$, 459s. ^{1}H NMR (400.13 MHz, DMSO-d_6, δ, ppm): 7.98–6.96 (m, 30H-Ph, 4H-sac), 4.17–4.04 (d, 2H, CH_2-benzyl, $^2J_{HP} = 12.0$ Hz), 3.89–3.82 (d, 2H, CH_2-benzyl, $^2J_{HP} = 12.0$ Hz). ^{13}C{^{1}H} NMR (100.62 MHz, DMSO-d_6, δ, ppm): 164.8 (s, C_7-sac), 139.6 (s, C_1-sac), 135.9 (s, $C_{para\text{-}Bz}$), 134.3 (d, $C_{ipso\text{-}Bz}$, $J_{PC} = 19.1$ Hz), 133.8 (s, $C_{ipso\text{-}Ph}$), 132.7 (d, $C_{meta\text{-}Ph}$, $J_{PC} = 10.1$ Hz), 132.4 (d, $C_{ortho\text{-}Ph}$, $J_{PC} = 11.1$ Hz), 130.4 (d, $C_{para\text{-}Ph}$, $J_{PC} = 4.0$ Hz), 130.3 (s, C_3-sac), 129.4 (d, $C_{ortho\text{-}Bz}$, $J_{PC} = 6.1$ Hz), 127.4 (s, C_6-sac), 127.0 (d, $C_{meta\text{-}Bz}$, $J_{PC} = 11.1$ Hz), 124.3 (s, C_4-sac), 124.0 (s, C_5-sac), 120.3 (s, C_2-sac), 30.9 (s, CH_2-Bz, *trans* to Cl), 28.0 (s, CH_2-Bz, *trans* to sac). ^{31}P{^{1}H} NMR (161.97 MHz, DMSO-d_6, δ, ppm): 14.9 (s, ^1JPtP = 2219.4 Hz). Molar conductivity, Λ_M (MeOH, 298 K, 1 mM) 7.9 S cm^2 mol^{-1} (nonelectrolyte). ESI-MS (m/z, MeOH): 988.1 (5%, calcd 988.3) $[M + Na]^+$, 783.7 (19%, calcd 783.2) $[M - sac]^+$, 746.9 (100%, calcd 746.7) $[Pt(PPh_2Bz)_2 - H]^+$.

4.3 | Hydrolysis and stability studies

The stock solutions of **3** and **4** (10^{-3} M) were prepared in a solution containing both DMSO and saline (1/9, v/v). In the hydrolysis studies, the UV–vis spectra of the 20 μM solutions were recorded at 298 K at 30 min intervals up to 240 min, while the spectra of the same solutions were also measured at 24 and 48 h to assess the solution stability of these complexes. The time-dependent ^{31}P spectra of **3** and **4** were also measured in neat DMSO at 0, 24 and 48 h.

4.4 | X-ray crystallography

The single-crystal XRD studies of **2–4** were performed using a Rigaku Oxford Xcalibur single-crystal X-ray diffractometer at rt with EOS CCD area detector using graphite-monochromated MoKα radiation ($\lambda = 0.71073$ Å) with ω-scan mode. The data collection, cell refinement and data reduction were performed using CrysAlis^{Pro} software v. 1.171.42.49.[62,63] Utilizing Olex2,[64] the structures were solved with the ShelXT structure solution program using Intrinsic Phasing[65] and refined with the ShelXL refinement package using least squares minimization.[66] All non-hydrogen atoms were refined with anisotropic thermal displacement parameters, while all hydrogen atoms were located at calculated positions and refined by using the riding model. The crystal structure of **3** was determined as a non-merohedral twin with a BASF value of 0.178 and the generation of the HKLF5 file in Olex2. The unit cell of the crystal structure of **2** has two voids ((0.0, 0.5, 0.5), 172.1 Å^3, 38.3 e−; (0.5, 0.0, 0.0), 172.1 Å^3, 38.3 e−) filled with disordered solvent molecules. The amount of electron density filling the voids shows that the disordered molecule in the voids is DMF, used in the synthesis process. The solvent masking procedure used by Olex2 was applied to remove electron densities in the voids. In addition, a number of DFIX/SADI/RIGU restraints and EADP constraints were applied to refine some disordered atoms or fragments of the molecular structures.

Crystallographic data are presented in Tables 1 and S1 and deposited at the Cambridge Crystallographic Data Centre with CCDC numbers 2288517–2288519. Copies of the data can be obtained free of charge via www.ccdc.cam.ac.uk/data_request/cif or by emailing data_request@ccdc.cam.ac.uk.

4.5 | Cell culture

HCT116 (colorectal cancer), HepG2 (hepatocellular cancer), A549 (non-small cell lung cancer), MDA-MB-231 (breast cancer), DU145 (prostate cancer), PANC-1 (pancreatic cancer), C6 (rat glioma) and BEAS-2B (normal bronchial epithelial cell) cells were cultured in RPMI 1640 medium (Gibco, Grand Island, NY, USA) supplemented with 100 U mL^{-1} penicillin + 100 μg mL^{-1} streptomycin (Gibco, Grand Island, NY, USA), 2 mM L-glutamine (Gibco, Grand Island, NY, USA), 10% foetal bovine serum (Lonza, Verviers, Belgium), at 37°C in a humidified atmosphere containing 5% CO_2.

4.6 | Cellular uptake studies

HCT116 cells were exposed to 10 μM of **2**, **4** and cisplatin at 37°C for 12 h. After removal of the incubation medium, the cells were washed with cold phosphate-buffered saline twice, trypsinized and eventually the number of cells in the suspension was counted. Three millilitres of ultrapure HNO_3 (69%) was added to the suspension, and the resulting solution was heated to dryness. The solid residue was then dissolved in 2 mL of HCl (37%) and heated to dryness to remove traces of HNO_3. The final residue was dissolved in 5 mL of double distilled water, and the Pt content of the solutions was determined by using an Agilent 7700 ICP-OES spectrometer and expressed as the mean of three measurements.

10990739, 0, Downloaded from https://onlinelibrary.wiley.com/doi/10.1002/aoc.7433 by Dokuz Eylul University, Wiley Online Library on [06/03/2024]. See the Terms and Conditions (https://onlinelibrary.wiley.com/terms-and-conditions) on Wiley Online Library for rules of use; OA articles are governed by the applicable Creative Commons License

4.7 | The SRB viability assay

In the SRB assay, cells were seeded in 96-well plate at the density of 5×10^3 cells/well and treated with the ligands, **1**–**4** and cisplatin for 48 h at different concentrations (at the range of 0.63–40 μM). Stock solutions of the compounds (40 mM each) were prepared in DMSO, and dilutions were made serially using cell culture medium so that the DMSO content did not exceed 0.1% in the final solutions. At the end of treatment, SRB assay measurements were carried out as previously described by Icsel et al.[67] The viability of treated cells was measured using the following equation in comparison with untreated control cells.

$$\text{Viability}\,(\%) = [100 \times (\text{Sample Abs})/(\text{Control Abs})].$$

4.8 | Flow cytometry assays

The colorectal cancer (HCT116) cells were seeded at 3×10^5 cells per well (in duplicate) into six-well plates and treated with IC_{75} doses of **4** (20 μM) and cisplatin (40 μM) for 12 and 24 h. For determination cell death-related parameters at the end of the treatment period, annexin V/Dead Cell (MCH100105, Millipore), caspase 3/7 activity (MCH100108, Millipore), ROS generation (MCH100111-2, Millipore), Bcl-2 inactivation (MCH200105, Millipore) and DNA damage (Phosphorylation of histone H2AX) (MCH200101, Millipore) were measured with a cell analyser (MUSE flow cytometry), according to the manufacturer's instructions.

4.9 | Evaluation of antiangiogenesis via CAM assay

Eggs were cleaned with 70% ethanol wiped towels and inspected using light to mark the air sacs on Egg Development Day 0 (EDD0). Then, the CAM membrane was dropped by drilling one hole in the air sac and another hole on the side. The eggs were then incubated upside down, so the hole where the old air sac was is at the bottom. On EDD3, approximately 3 mL of albumin was drawn from the eggs. On EDD4, the tops of the eggs were opened and sealed with film. The eggs were incubated at 37°C and 70% humidity. On EDD5, **4** was applied to the CAM layer by impregnating sterile wafers of 0.5 cm diameter at a dose of 50 ng per egg. Thalidomide was used as a positive control at a dose of 50 μg per egg.[58] The development of the vessels was tracked by photographing on EDD5 and EDD6. Each test was performed in triplicate. The antiangiogenic effect score on vascular development was calculated using the following equation.[61]

$$\text{Average Score} = \frac{(\text{Score 2})\,\text{egg count} \times 2 + (\text{Score 1})\,\text{egg count}}{\text{Total number of eggs scored}}.$$

Score <0.5 = no antiangiogenic effect, 0.5–0.75 = weak antiangiogenic effect, 0.75–1 = good antiangiogenic effect and >1 = strong antiangiogenic effect.

ACKNOWLEDGEMENTS

We thank Professor I. Ozdemir of Inonu University for the NMR measurements, and Professor D. Ozdes of Gümüşhane University for the determination of the Pt contents of the cell material.

CONFLICT OF INTEREST STATEMENT

The authors declare no conflict of interest.

DATA AVAILABILITY STATEMENT

The data that support the findings of this study are available in the Supporting Information.

ORCID

Ceyda Icsel https://orcid.org/0000-0002-2717-2430
Veysel T. Yilmaz https://orcid.org/0000-0002-2849-3332
Muhittin Aygun https://orcid.org/0000-0001-9670-9062
Merve Erkisa https://orcid.org/0000-0002-3127-742X
Engin Ulukaya https://orcid.org/0000-0003-4875-5472
R. Okan Akar https://orcid.org/0000-0001-8687-2034

REFERENCES

[1] E. J. Baran, V. T. Yilmaz, *Coord. Chem. Rev.* **2006**, *250*, 1980.
[2] S. Medici, M. Peana, V. M. Nurchi, J. I. Lachowicz, G. Crisponi, M. A. Zoroddu, *Coord. Chem. Rev.* **2015**, *284*, 329.
[3] M. Fanelli, M. Formica, V. Fusi, L. Giorgi, M. Micheloni, P. Paoli, *Coord. Chem. Rev.* **2016**, *310*, 41.
[4] V. Brabec, O. Hrabina, J. Kasparkova, *Coord. Chem. Rev.* **2017**, *351*, 2.
[5] L. Cai, C. Yu, L. Ba, Q. Liu, Y. Qian, B. Yang, C. Gao, *Appl. Organomet. Chem.* **2018**, *32*, e4228.
[6] K. M. Deo, D. L. Ang, B. McGhie, A. Rajamanickam, A. Dhiman, A. Khoury, J. Holland, A. Bjelosevic, B. Pages, C. Gordon, J. R. Aldrich-Wright, *Coord. Chem. Rev.* **2018**, *375*, 148.
[7] K. Peng, B.-B. Liang, W. Liu, Z.-W. Mao, *Coord. Chem. Rev.* **2021**, *449*, 214210.
[8] R. Czarnomysy, D. Radomska, O. K. Szewczyk, P. Roszczenko, K. Bielawsk, *Int. J. Mol. Sci.* **2021**, *22*, 8271.
[9] R. Sharma, V. J. Singh, P. A. Chawla, *Anti-Cancer Agents Med. Chem.* **2022**, *22*, 821.
[10] P. Starha, R. Krikavova, *Coord. Chem. Rev.* **2024**, *501*, 215578.
[11] M. N. Alam, F. Huq, *Coord. Chem. Rev.* **2016**, *316*, 36.
[12] M. Vojtek, M. P. M. Marques, I. M. P. L. V. O. Ferreira, H. Mota-Filipe, C. Diniz, *Drug Discov. Today* **2019**, *24*, 1044.

10990739, 0, Downloaded from https://onlinelibrary.wiley.com/doi/10.1002/aoc.7433 by Dokuz Eylul University, Wiley Online Library on [06/03/2024]. See the Terms and Conditions (https://onlinelibrary.wiley.com/terms-and-conditions) on Wiley Online Library for rules of use; OA articles are governed by the applicable Creative Commons License

[13] T. Scattolin, V. A. Voloshkin, F. Visentin, S. P. Nolan, *Cell Rep.* **2021**, *2*, 100446.
[14] M. Cavicchioli, A. C. Massabni, E. E. Castellano, L. P. B. Sabeh, C. M. Costa-Neto, *Inorg. Chim. Acta* **2007**, *360*, 3055.
[15] S. A. Al-Jibori, G. H. Al-Jibori, L. J. Al-Hayaly, C. Wagner, H. Schmidt, S. Timur, F. B. Barlas, E. Subasi, S. Ghosh, G. Hogarth, *J. Inorg. Biochem.* **2014**, *141*, 55.
[16] E. Guney, V. T. Yilmaz, F. Ari, O. Buyukgungor, E. Ulukaya, *Polyhedron* **2011**, *30*, 114.
[17] F. Ari, N. Aztopal, C. Icsel, V. T. Yilmaz, E. Guney, O. Buyukgungor, E. Ulukaya, *Bioorg. Med. Chem.* **2013**, *21*, 6427.
[18] E. Ulukaya, F. Ari, K. Dimas, M. Sarimahmut, E. Guney, N. Sakellaridis, V. T. Yilmaz, *J. Cancer Res. Clin. Oncol.* **2011**, *137*, 1425.
[19] E. I. Ikitimur-Armutak, K. Sonmez, K. Akgun-Dar, G. Sennazli, A. Kapucu, F. Yigit, V. T. Yilmaz, E. Ulukaya, *Anticancer Res* **2015**, *35*, 1491.
[20] Y. Cetin, Z. Adiguzel, H. U. Polat, T. Akkoc, A. Tas, B. Cevatemre, G. Celik, B. Carikci, V. T. Yilmaz, E. Ulukaya, C. Acilan, *Anticancer Drugs* **2017**, *28*, 898.
[21] R. Paprocka, M. Wiese-Szadkowska, S. Janciauskiene, T. Kosmalski, M. Kulik, *Coord. Chem. Rev.* **2022**, *452*, 214307.
[22] W. Henderson, B. K. Nicholson, L. J. McCaffrey, *Inorg. Chim. Acta* **1999**, *285*, 145.
[23] V. T. Yilmaz, C. Icsel, O. R. Turgut, M. Aygun, M. Erkisa, M. H. Turkdemir, E. Ulukaya, *Eur. J. Med. Chem.* **2018**, *155*, 609.
[24] C. Icsel, V. T. Yilmaz, B. Cevatemre, M. Aygun, E. Ulukaya, *J. Inorg. Biochem.* **2019**, *195*, 39.
[25] C. Icsel, V. T. Yilmaz, B. Cevatemre, M. Aygun, E. Ulukaya, *J. Biol. Inorg. Chem.* **2020**, *25*, 75.
[26] C. Icsel, V. T. Yilmaz, M. Aygun, E. Ulukaya, *Bioorg. Med. Chem. Lett.* **2020**, *30*, 127077.
[27] C. Icsel, V. T. Yilmaz, M. Aygun, B. Cevatemre, P. Alper, E. Ulukaya, *Dalton Trans.* **2018**, *47*, 11397.
[28] V. T. Yilmaz, C. Icsel, M. Aygun, M. Erkisa, E. Ulukaya, *Eur. J. Med. Chem.* **2018**, *158*, 534.
[29] S. J. Berners-Price, P. J. Sadler, *Bioinorganic Chemistry. Structure and Bonding*, Vol. 70, Springer, Berlin, Heidelberg **1988** 27.
[30] P. Vafopoulou, M. Kourti, *J. Cancer Met. Treat.* **2022**, *8*, 18.
[31] C. Icsel, *Turk. J. Chem.* **2020**, *44*, 736.
[32] G. Binev, A. B. Stamboliyska, E. A. Velcheva, *Spectrochim. Acta A* **1996**, *A52*, 1135.
[33] L. Rigamonti, C. Manassero, M. Rusconi, M. Manassero, A. Pasini, *Dalton Trans.* **2009**, *7*, 1206.
[34] Z. Kokan, B. Peric, G. Kovacevic, A. Brozovic, N. Metzler-Nolte, S. I. Kirin, *Eur. J. Inorg. Chem.* **2017**, *2017*, 3928.
[35] V. T. Yilmaz, C. Icsel, O. R. Turgut, M. Aygun, E. Evren, I. Ozdemir, *Inorg. Chim. Acta* **2020**, *500*, 119220.
[36] V. A. Stepanova, L. M. Egan, L. Stahl, I. P. Smoliakova, *J. Organomet. Chem.* **2011**, *696*, 3162.
[37] A. Tolman, *Chem. Rev.* **1977**, *77*, 313.
[38] Z. D. Bugarcic, J. Bogojeski, R. van Eldik, *Coord. Chem. Rev.* **2015**, *292*, 91.
[39] A. Leo, C. Hansch, D. Elkins, *Chem. Rev.* **1971**, *71*, 525.
[40] E. Rutkowska, K. Pajak, K. Jozwiak, *Acta Pol. Pharm.* **2013**, *70*, 3.
[41] S. P. Oldfield, M. D. Hall, J. A. Platts, *J. Med. Chem.* **2007**, *50*, 5227.
[42] I. V. Tetko, H. P. Varbanov, M. Galanski, M. Talmaciu, J. A. Platts, M. Ravera, E. Gabano, *J. Inorg. Biochem.* **2016**, *156*, 1.
[43] G. Natile, M. Coluccia, *Coord. Chem. Rev.* **2001**, *216–217*, 383.
[44] U. Kalinowska-Lis, J. Ochocki, K. Matlawska-Wasowska, *Coord. Chem. Rev.* **2008**, *252*, 1328.
[45] S. M. Aris, N. P. Farrell, *Eur. J. Inorg. Chem.* **2009**, *10*, 1293.
[46] A. G. Quiroga, *J. Inorg. Biochem.* **2012**, *114*, 106.
[47] G. Koopman, C. P. Reutelingsperger, G. A. Kuijten, R. M. Keehnen, S. T. Pals, M. H. van Oers, *Blood* **1994**, *84*, 1415.
[48] I. Budihardjo, H. Oliver, M. Lutter, X. Luo, X. Wang, *Annu. Rev. Cell Dev. Biol.* **1999**, *15*, 269.
[49] J. E. Chipuk, D. R. Green, *Trends Cell Biol.* **2008**, *18*, 157.
[50] X. Li, Y. Wang, M. Li, H. Wang, X. Dong, *Molecules* **2021**, *27*, 148.
[51] U. S. Srinivas, B. W. Q. Tan, B. A. Vellayappan, A. D. Jeyasekharan, *Redox Biol.* **2019**, *25*, 101084.
[52] L. J. Kuo, L. X. Yang, *In Vivo* **2008**, *22*, 305.
[53] V. Turinetto, C. Giachino, *Nucleic Acids Res.* **2015**, *43*, 2489.
[54] R. Schneider-Stock, D. Ribatti, *Handb. Exp. Pharmacol.* **2021**, *265*, 303.
[55] D. Ribatti, *Exp. Cell Res.* **2021**, *400*, 112510.
[56] J. Dürig, M. Calcagni, J. Buschmann, *Mater. Today Bio.* **2023**, *22*, 100757.
[57] E. I. Ikitimur-Armutak, E. Gurel-Gurevin, H. T. Kiyan, S. Aydinlik, V. T. Yilmaz, K. Dimas, E. Ulukaya, *Microvasc. Res.* **2017**, *109*, 26.
[58] S. Aydinlik, A. Uvez, H. T. Kiyan, E. Gurel-Gurevin, V. T. Yilmaz, E. Ulukaya, E. I. Armutak, *Microvasc. Res.* **2021**, *138*, 104229.
[59] R. J. D'Amato, M. S. Loughnan, E. Flynn, J. Folkman, *Proc. Natl. Acad. Sci. U. S. A.* **1994**, *91*, 4082.
[60] A. Mercurio, G. Adriani, A. Catalano, A. Carocci, L. Rao, G. Lentini, M. M. Cavalluzzi, C. Franchini, A. Vacca, F. Corbo, *Curr. Med. Chem.* **2017**, *24*, 2736.
[61] L. Krenn, D. H. Paper, *Phytomedicine* **2009**, *16*, 1083.
[62] *CrysAlisPro Software System, V1.171.41.49*, Rigaku Corporation, Oxford, UK **2022**.
[63] R. C. Clark, J. S. Reid, *Acta Crystallogr., Sect. A: Found. Crystallogr.* **1995**, *51*, 887.
[64] O. V. Dolomanov, L. J. Bourhis, R. J. Gildea, J. A. K. Howard, H. Puschmann, *J. App. Crystallogr.* **2009**, *42*, 339.
[65] G. M. Sheldrick, *Acta Crystallogr. Sect. A: Found. Adv.* **2015**, *71*, 3.
[66] G. M. Sheldrick, *Acta Crystallogr. Sec. C Struct. Chem.* **2015**, *71*, 3.
[67] C. Icsel, V. T. Yilmaz, M. Aygun, M. Erkisa, E. Ulukaya, *Dalton Trans.* **2023**, *52*, 7048.

SUPPORTING INFORMATION

Additional supporting information can be found online in the Supporting Information section at the end of this article.

How to cite this article: C. Icsel, V. T. Yilmaz, M. Aygun, M. Erkisa, E. Ulukaya, R. O. Akar, *Appl Organomet Chem* **2024**, e7433. https://doi.org/10.1002/aoc.7433

10990739, 0, Downloaded from https://onlinelibrary.wiley.com/doi/10.1002/aoc.7433 by Dokuz Eylul University, Wiley Online Library on [06/03/2024]. See the Terms and Conditions (https://onlinelibrary.wiley.com/terms-and-conditions) on Wiley Online Library for rules of use; OA articles are governed by the applicable Creative Commons License